Journal of Atmospheric and Terrestrial Physics, Vol. 48, No. 5, pp. 471–483, 1986.
Printed in Great Britain.

0021-9169/86 $3.00 + .00
Pergamon Journals Ltd.

The *E*-region electron density diurnal asymmetry at Saint-Santin: observations and role of nitric oxide

J.-CL. GÉRARD
Institut d'Astrophysique, University of Liège, B-4200 Cointe-Liège, Belgium

and

C. TAIEB
CNRS/CNET/CRPE, F-92131 Issy-les-Moulineaux, France

(*Received in final form* 2 *December* 1985)

Abstract—Measurements of the *E*-region electron density were made with the Saint-Santin incoherent scatter radar during consecutive days in June 1978, March 1979 and December 1980. On the basis of a statistical study, the observations show the presence of a diurnal asymmetry of the electron density, with morning values usually exceeding the afternoon densities by 3–20%. Two possible causes of the dissymmetry are examined: the asymmetry in the diurnal variation of the neutral composition and the effect of nitric oxide. The presence of NO partly converts O_2^+ into NO^+ ions and increases the effective recombination rate of the electrons in the afternoon. Numerical simulations assessing the relative importance of the two factors are, in general, in good agreement with the measurements.

1. INTRODUCTION

The existence of an asymmetry about local noon in the diurnal variation of the *E*-region critical frequency f_0E in ionograms has been discussed by APPLETON and LYON (1961), who analysed series of ionograms obtained at various latitudes and seasons. They concluded that the f_0E maximum is usually shifted a few minutes after local noon, except at low latitudes, where the peak generally precedes noon. APPLETON (1953) ascribed these lags between the *E*-region peak density and local noon to the 'sluggishness' of the ionosphere, i.e. to the time constant introduced by the characteristic time of electron recombination $(2\alpha N_0)^{-1}$, where α is the effective recombination coefficient and N_0 the maximum electron density. However, laboratory determinations of the recombination coefficient of major molecular ions indicated that these time constants are too small to introduce a measurable phase lag between the ionization function and the electron concentration. The derivation of the maximum *E*-region electron density from ionograms is complicated by the frequent presence of additional cusps, corresponding to additional sporadic *E* stratification. These effects make it difficult to determine unambiguously the f_0E value or to give it a clear physical significance.

Progress on this question was made with the use of incoherent scatter radar facilities able to measure the electron concentration at fixed altitude. Using this technique, MONRO *et al.* (1976) described the diurnal variation of electron density between 95 and 120 km measured from Saint-Santin in 1969 and 1970. They illustrated their study with the measurements of 28 April and 21 July 1970. Both days exhibited a diurnal asymmetry, with morning values generally exceeding the afternoon values. By comparing the measurements with an ionospheric model, they concluded that the asymmetries are produced by atmospheric tides, which induce temperature and density changes. In particular, they calculated that the total density and the chemical composition changes during the day produce the observed effect and tend to yield large morning electron concentrations. They indicated that vertical ion drift plays a negligible role in the lower *E*-region and contributes only a few per cent in the electron continuity equation at 120 km.

FORBES (1981) examined the role of diurnal and semidiurnal oscillations in temperature and O_2, N_2 and O densities as a source of *D*- and *E*-region diurnal asymmetries. He noted that the local changes in atmospheric densities are accompanied by simultaneous readjustments of the optical depth of the overlying atmosphere. His model calculations indicated that at 120 km the increase of the column density overshadows the local density variation and tends to produce larger electron concentrations in the afternoon with the phase function he adopted.

The potential role of nitric oxide in the ionospheric asymmetry was suggested by SENIOR *et al.* (1981).

Their work was initiated by a study of the diurnal variation of the *E*-region conductivities over Saint-Santin. The measurements indicated systematically smaller values in the afternoon than in the morning for equal solar zenith angles. They ascribed this effect to electron density asymmetry, which they attributed to nitric oxide through the charge transfer reaction

$$O_2^+ + NO \rightarrow NO^+ + O_2.$$

Since the ion recombination coefficient for NO^+ is larger than that for O_2^+, electrons recombine faster when the $[NO^+]/[O_2^+]$ ratio is large, which occurs when the NO density increases.

Model calculations and satellite observations (STEWART and CRAVENS, 1978) indicate that the lower thermospheric NO diurnal variation is asymmetric with respect to noon, with maximum concentrations observed in the early afternoon. This mechanism would thus be able to explain larger morning electron concentrations. SENIOR *et al.* (1981) formulated a third-order algebraic equation giving the steady-state electron density as a function of the local NO concentration. They found that the asymmetry is maximum for NO densities between 10^7 and $10^8\,cm^{-3}$.

The purpose of this paper is to describe the results of three series of measurements of the diurnal variation of N_e made from Saint-Santin on consecutive days at different seasons and discuss their statistical significance. The relative importance of the variation of major neutral constituents and nitric oxide is examined quantitatively with numerical models of the ionosphere and odd nitrogen.

2. SAINT-SANTIN MEASUREMENTS

The incoherent scatter facility at Saint-Santin is a tristatic radar measuring electron temperature (T_e), ion temperature (T_i), electron density (N_e) and three components of the ion velocity in the ionosphere above a point located at 44.65°N latitude and 2.15°E longitude. These parameters are obtained from the received signal scattered from the volume at the intersection of the receiving and transmitting antennas. The size of the volume is about 3 km height in the *E*-region and the altitudes of measurement are 100, 105, 110 and 120 km.

The electron density profile, including points in the *F*-region, is obtained in 45 min, which is the time interval for each measurement. With the 3 min integration time of the received signal, the experimental error for the electron density measurements is approximately 2%.

The periods of observation are 1–14 June 1978, 21–30 March 1979 and 9–18 December 1980. These periods were selected because they provide 3 sets of consecutive days at different seasons, allowing a statistical study of each period to be made.

The June 1978 period (Table 1) is characterized by fairly active conditions during the first half of the period. The *Ap* index reaches values of 82 and 38 and 2 and 5 June, respectively. The second part of the period is fairly quiet. The early June magnetic storm and its effects on *F*-region ion drift have recently been described by MAZAUDIER and BERNARD (1985). March 1979 was a moderately disturbed period, with a magnetic storm developing on 22 March (average *Ap* index 26). The December 1980 measurements were made during fairly quiet conditions, with the *Ap* index never exceeding 16 (average *Ap* index 11). The 10.7 cm solar flux was steadily increased from rather low solar activity in 1978 to values typical of the maximum of cycle 21 in December 1980 (average $F_{10.7}$ flux 232).

As an example of the observations, in Fig. 1 N_e measured on 12 June 1978 has been plotted as a function of cos χ, where χ is the solar zenith angle from about 05.00 to 17.45 LT. for 105, 110 and 120 km. This plot exhibits differences between morning and afternoon values for the same cos χ. The time range of the observations depends on the duration of daylight and, consequently, on the season. The minimum electron density detectable is not less than $1 \times 10^4\,cm^{-3}$. For cos $\chi = 0.70$, the morning electron density is larger than the afternoon by 10% at 105 km, 5% at 110 km and 8% at 120 km. Once the daily variation of electron densities versus cos χ has been established and spurious data points have been removed, a statistical analysis of the diurnal variation is performed.

Table 1. Geophysical characteristics for the days of the June 1978 measurements

Date (June 1978)	$F_{10.7}$ ($10^{-22}\,W\,m^{-2}\,Hz^{-1}$)	*Ap*
1	149.1	9
2	147.0	82
3	130.8	31
4	118.6	26
5	116.9	38
6	109.8	8
7	110.6	11
8	109.3	10
9	106.5	4
10	108.4	24
11	113.2	17
12	116.4	10
13	120.3	7
14	126.4	4

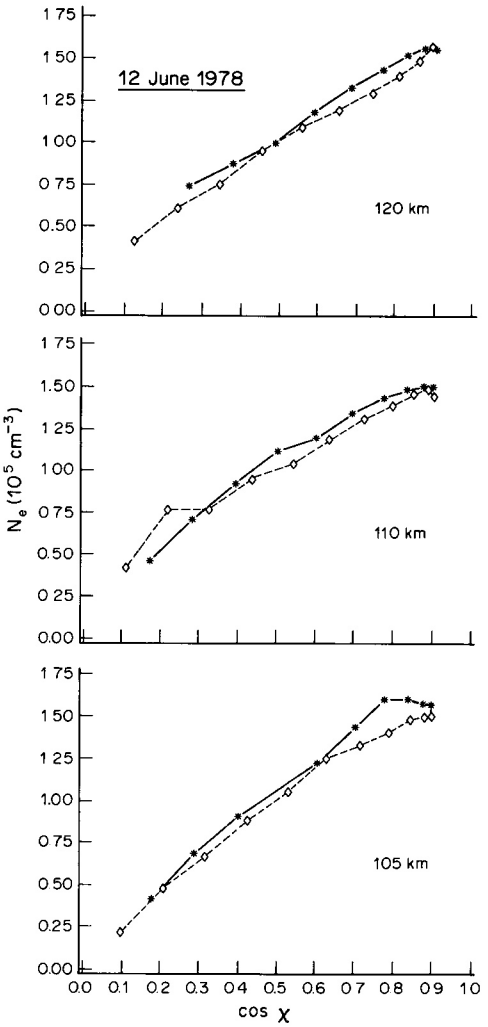

Fig. 1. Plot of electron density measured on 12 June 1978 versus cos χ at three different altitudes. The solid lines indicate morning measurements, dashed lines afternoon measurements.

The set of observations considered for this analysis may be one day or a whole period of consecutive days, as will be discussed below. Practically, a density ratio R_i at a given altitude is obtained by dividing each morning concentration by the linearly interpolated afternoon value corresponding to the same solar zenith angle. The mean ratio of the set is then

$$\bar{R} = \sum_i R_i / N$$

and its standard deviation is given by

$$\sigma_R = \frac{\sqrt{\sum (R_i - \bar{R})^2}}{(N-1)},$$

where N is the number of individual ratios. The difference $d = \bar{R} - 1$ is then compared to σ_R to determine whether the average morning to afternoon density ratio is significantly different from 1. In this discussion we adopt $d = 2\sigma_R$ as a confidence interval, corresponding to a 95% confidence coefficient. Figure 2 summarizes the variation of the diurnal asymmetry for the observations of June 1978.

It exhibits the daily values of $\bar{R}$ at three different altitudes during this period. It shows that at all 3 altitudes the density ratio is usually larger than 1, with substantial day-to-day variations. Although most ratios are within 10% of unity, considerably larger values are observed during 7 and 8 June. Figure 3 shows the measurements made on 7 June 1978 at 120, 110 and 105 km. Values of the dissymmetry ratio as large as 1.45 are obtained at 105 and 110 km. As can be seen in Fig. 2, the behaviour of the *E*-region on this day is characterized by a very large morning–afternoon dissymmetry, exceeding by far typical values of a few per cent usually observed. Also apparent in this figure is the noon minimum at all three altitudes. Such a minimum has been observed previously at Slough by APPLETON and LYON (1961) on plots of f_0E critical frequency versus local time. After this period, the ratios return to normal values slightly larger than unity. Values smaller than 1 are also occasionally observed, especially at 105 km. The smallest ratio for this period is equal to 0.96 and was obtained on 11 June.

The global statistical results for the 3 periods of measurements are summarized in Table 2. Column 3 indicates the number of individual ratios. Column 4 confirms that for June 1978 the assymmetry reaches globally 11%, 7% and 9%, respectively, at 105, 110 and 120 km and $\bar{R}$ is significantly larger than unity for this period. In contrast, no significant asymmetry

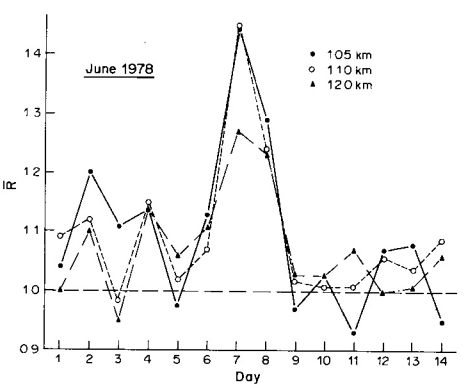

Fig. 2. Average daily dissymmetry ratio for the June 1978 period of observations at three different altitudes.

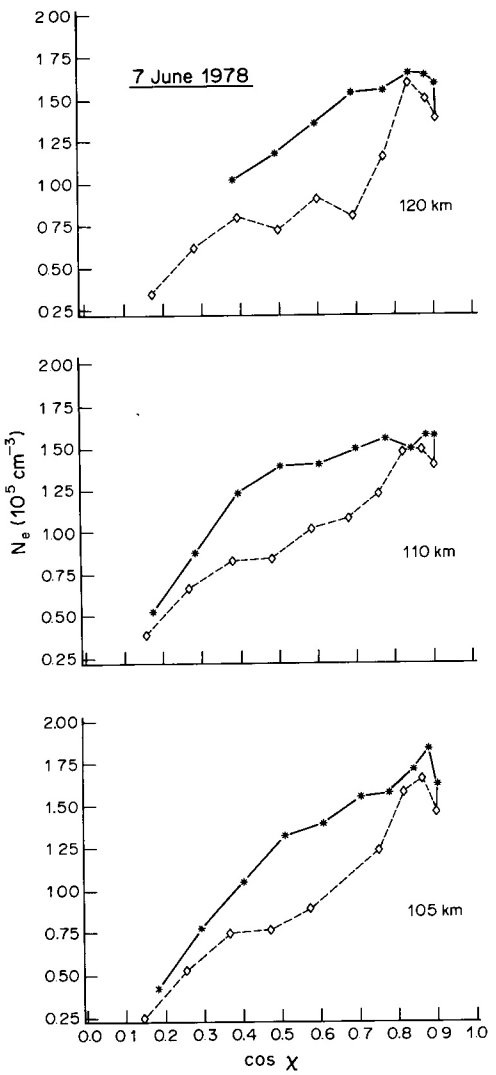

Fig. 3. As Fig. 1 for 7 June 1978.

exists for the March 1979 period, although some individual days exhibit this effect. The average ratios are 1.19 and 1.06 at 100 and 120 km, respectively, during the December 1980 measurements and thus, this period also shows significantly larger electron densities during morning hours. It may be concluded that the June 1978 and the December 1980 periods show significant diurnal asymmetries of the *E*-region, whereas the March 1979 measurements show no statistical evidence of this effect. However, individual days of all three periods occasionally show a behaviour different from the average, including days with reversed asymmetry.

3. MODEL DESCRIPTION

SENIOR *et al.* (1981) have suggested that the morning–afternoon *E*-region dissymmetry is mainly due to the presence of nitric oxide in the lower thermosphere. Neglecting the transport term in the continuity equation for O_2^+, N_2^+ and NO^+ and solving for N_e and [NO], they obtained the polynomial equation

$$AN_e^3 + B[\mathrm{NO}]N_e^2 - CN_e - D[\mathrm{NO}] = 0,$$

where [NO] is the concentration of NO and A, B, C, D are constants which depend on the recombination coefficients of Table 3 and ion production rates:

$$A = \alpha_2\alpha_4; \quad B = \alpha_4\alpha_5;$$

$$C = \alpha_4 P(O_2^+) + \alpha_2 P(N_2^+);$$

$$D = \alpha_5[P(O_2^+) + P(N_2^+)].$$

P_i denote the individual ion production rates due to EUV solar flux. When [NO] is increased from

Table 2. Statistical results of the measured electron density dissymmetry

Period	Altitude	N	$\bar{R}$	$2\sigma_R$
1–14 June 1978	105	114	1.11	0.05
	110	117	1.07	0.03
	120	103	1.09	0.04
21–30 March 1979	105	56	0.99	0.02
	110	55	0.99	0.04
	120	49	1.01	0.07
9–18 December 1980	100	45	1.19	0.10
	120	32	1.06	0.06

Table 3. Chemical reactions and rate coefficients used in the models

Process	Reaction	Rate coefficient ($cm^3 s^{-1}$)
Recombination	$O^+ + e \rightarrow O + h\nu$	$\alpha_1 = 2.0 \times 10^{-12}(250/T_e)^{0.7}$
	$O_2^+ + e \rightarrow O + O$	$\alpha_2 = 2.2 \times 10^{-7}(300/T_e)$
	$N_2^+ + e \rightarrow N(^4S) + N(^2D)$	$\alpha_3 = 1.8 \times 10^{-7}(300/T_e)^{1/3}$
	$NO^+ + e \rightarrow N(^4S, ^2D) + O$	$\alpha_4 = 4.1 \times 10^{-7}(300/T_e)$
Charge exchange	$O^+ + N_2 \rightarrow O + N_2^+$	$\gamma_1 = 1.0 \times 10^{-10}$
	$O^+ + N_2 \rightarrow N + NO^+$	$\gamma_2 = 1.53 \times 10^{-12} - 5.92 \times 10^{-13}(T_n/300)$
	$O^+ + O_2 \rightarrow O + O_2^+$	$\gamma_3 = 2.82 \times 10^{-11} - 7.74 \times 10^{-12}(T_n/300)$
	$O^+ + NO \rightarrow O + NO^+$	$\gamma_4 = 1.53 \times 10^{-12} - 5.92 \times 10^{-13}(T_n/300)$
	$O_2^+ + NO \rightarrow O_2 + NO^+$	$\gamma_5 = 4.4 \times 10^{-10}$
	$O_2^+ + N_2 \rightarrow NO + NO^+$	$\gamma_6 = 2.0 \times 10^{-16}$
	$N_2^+ + O_2 \rightarrow NO + NO^+$	$\gamma_7 = 3.0 \times 10^{-14}$
	$N_2^+ + O \rightarrow N(^2D) + NO^+$	$\gamma_8 = 1.4 \times 10^{-10}(300/T_n)^{0.44}$
	$N_2^+ + O_2 \rightarrow N_2 + O_2^+$	$\gamma_9 = 7.0 \times 10^{-11}$
	$N_2^+ + NO \rightarrow N_2 + NO^+$	$\gamma_{10} = 3.3 \times 10^{-10}$
	$N_2^+ + O \rightarrow N_2 + O^+$	$\gamma_{11} = 1.0 \times 10^{-12}(300/T_n)^{0.23}$
Odd nitrogen reactions	$NO + h\nu \rightarrow N(^4S) + O$	$J_{NO}(s^{-1})$
	$N(^4S) + O_2 \rightarrow NO + O$	$\gamma_{12} = 4.4 \times 10^{-12} \exp(-3220/T_n)$
	$N(^2D) + O_2 \rightarrow NO + O$	$\gamma_{13} = 6 \times 10^{-12}$
	$N(^2D) + e \rightarrow N(^4S) + e$	$\gamma_{14} = 5.5 \times 10^{-10}(300/T_e)^{-0.5}$
	$N(^2D) + O \rightarrow N(^4S) + O$	$\gamma_{15} = 5 \times 10^{-13}$
	$N(^2D) \rightarrow N(^4S) + h\nu$	$\gamma_{16} = 1.07 \times 10^{-5}(s^{-1})$
	$N(^4S) + NO \rightarrow N_2 + O$	$\gamma_{17} = 3.4 \times 10^{-11}$
	$N(^2D) + NO \rightarrow N_2 + O$	$\gamma_{18} = 7 \times 10^{-11}$

5×10^7 cm^{-3} to 10^8 cm^{-3}, the electron density decreases by about 10%. They also showed that for [NO] values outside the range 10^7–10^8 cm^{-3}, the effect is sharply reduced.

This first approach to evaluate the effect of NO is simplified, since no account has been taken of the diurnal variation of temperature and concentration of the neutral constituents or the real variation of NO density. In order to assess the relative role of NO and neutral composition changes, it is necessary to model quantitatively both the diurnal variation of NO and of the neutral and ion species.

3.1. *Ionospheric model*

The recent model of the ionosphere by TAIEB and POINSARD (1984a) has been used to simulate how the neutral atmosphere contributes to the asymmetry. The mathematical method for solving the differential equations is a 'spectral method' providing the solution as a 50 coefficients polynomial with a grid irregularly spaced between 100 and 600 km so that altitudes of measurement do not coincide with the grid altitudes.

The model that describes the concentration of profiles O_2^+, N_2^+, O^+ and NO^+ include three physical phenomena: production, loss by chemical reactions and transport of the ions and electrons.

For the calculation of production due to photoionisation by solar UV radiation, absorption and ionisation coefficients are the same as the coefficients used by TAIEB and POINSARD (1984a). The main ionospheric reactions are listed in Table 3. The solar spectrum 78348 given by TORR *et al.* (1979) linearly scaled to the actual $F_{10.7}$ index is adopted.

The loss by recombination of ions with electron depends on electron temperature (T_e), while the loss by charge exchange depends on neutral temperature (T_n). The electron temperature is derived from the empirical model of PANDEY and MAHAJAN (1981), which includes the dependence on electron density. The ion temperature is taken as equal to the neutral temperature.

In the *E*-region, where collision frequency is larger than ion gyrofrequency, ions are moved horizontally by neutral drag and the electric field, as far as a vertical gradient of neutral wind does not exist. Such gradients are partly responsible for sporadic *E* formation. Otherwise, when the only forces are neutral drag and the electric field, the plasma moves horizontally and there is no change in the vertical distribution of the ionisation. In these circumstances, the transport term of the continuity equations can be neglected.

The boundary value at 100 km for each ion is based on the assumption that N_2^+ and O^+ concentrations are less than 1% of O_2^+ and NO^+ concentrations and that $N_e = [O_2^+] + [NO^+]$. At 100 km N_e is a measured value at the initial time and changes according to observations as a function of cos χ. At the upper boundary the slope of the N_e profile is an experimental

value, in the same way as explained in Taieb and Poinsard (1984a).

To start the integration with realistic initial values of the concentration profiles, the simulation runs for 24 h from 0.500 UT. Then, starting again with the profiles so obtained, the simulation runs again with 3 min time-steps until 20.00 UT.

All physical phenomena depend on neutral concentration and their temperature (T_n), which are provided by the revised MSIS-83 model (Hedin, 1983). The conditions of the model are controlled by Ap, the $F_{10.7}$ solar flux and the mean value of the $F_{10.7}$ flux over 30 days before 10 June 1978. The chemical effects of nitric oxide on ionospheric composition are included, based on the results of a time-dependent NO model. This odd nitrogen model is described below and calculated odd nitrogen densities are compared with satellite measurements. The diurnal NO variation over Saint-Santin is then described and used as a guide to the numerical simulations with the ionospheric model.

3.2. *The nitric oxide time-dependent model*

Description and comparison with satellite measurements. The model used to predict nitric oxide diurnal variation is based on the model described by Cravens *et al.* (1980), with some modifications. A description is given in the Appendix.

Before using it to calculate the diurnal variation of NO over Saint-Santin, its validity is demonstrated by comparing the calculated odd nitrogen concentrations with simultaneous measurements of the largest possible number of odd nitrogen species. An opportunity was provided by the observations made near perigee of the AE-C orbit 594. During this period the instruments measured electron and neutral temperatures, the concentrations of positive ions and the densities of O, N_2, $N(^2D)$ and NO above 150 km (Rusch *et al.*, 1975). Although not usually available, the $N(^4S)$ density could be deduced from the Neutral Atmosphere Composition Experiment (NACE) by Carignan and Rusch (cf. Torr and Torr, 1982). The observations were made on 18 February 1974 near 39°N at 5.24 UT during a solar and geomagnetically quiet period ($F_{10.7} = 79, Ap = 12$).

The model was run for several simulated days with different combinations of values for K and f and values of Ap and $F_{10.7}$ indices appropriate to the day of the observations. The branching ratio f was varied from 0.6 to 0.8 and the eddy diffusion coefficient K from Ebel (1980) and Oran *et al.* (1975) were used for comparison.

Figure 4 illustrates the comparison between the calculated odd nitrogen concentrations and the values measured on upleg and downleg. As expected, when the branching ratio f is increased from 0.6 to 0.8 (cases 1 and 2), the $N(^2D)$ concentration increases by about 15%. This change of branching ratio has little influence on the NO density above 150 km, since reaction γ_{12} provides the major source of nitric oxide in this region. However, a nearly two-fold increase is obtained for the peak concentration and the altitude of the maximum decreases by about 6 km when f is

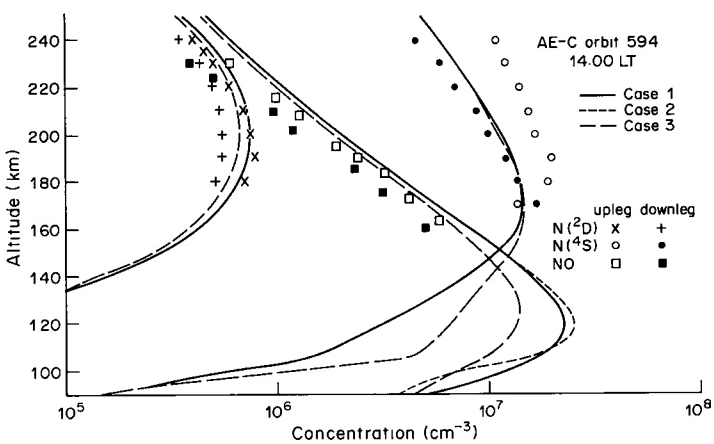

Fig. 4. Vertical distribution of odd nitrogen species calculated for the conditions of AE-C orbit 584 perigee. The concentrations measured on downleg and upleg are represented by different symbols. Case 1 corresponds to a branching ratio $f = 0.8$ and Ebel's K profile; case 2, $f = 0.8$ and low K profile (see text); case 3, $f = 0.6$ and Ebel's K coefficient.

increased to 0.8. If the eddy diffusion coefficient is decreased (case 2), no noticeable effect is seen on atomic nitrogen. A small increase of the NO peak is obtained, together with a decrease below 108 km caused by the reduced downward flux associated with the smaller K. Considering experimental errors associated with the three different instruments, possible latitudinal concentration gradients and uncertainties in the model, all 3 cases satisfactorily match the observations. The calculated high altitude NO concentration tends in all cases to be about 50% higher than the measurements. However, O_2 density was not measured by the neutral mass spectrometer and the MSIS O_2 concentration used for this calculation is 49% higher at 200 km than the O_2 deduced by RUSCH *et al.* (1975) from the O^+/O_2^+ ratio, whereas the O and N_2 MSIS densities agree with the measurements within 10%. Consequently, it may be concluded that this NO model satisfactorily matches the observations. Then we apply it to the calculation of the NO diurnal variation at Saint-Santin latitude.

Nitric oxide diurnal variation over Saint-Santin. The model described above was run for the latitude of Saint-Santin parameters (Ap 20, $F_{10.7}$ 117) appropriate to the June 1978 period. The result of the calculation of NO diurnal variation is shown in Fig. 5. It shows an E-region peak near 115 km at 15.00 LT reaching a maximum $4\times10^7\,\mathrm{cm}^{-3}$ and a minimum of about 2×10^7 near 7.00 LT. The depth of the mesospheric dip near 85 km is also time-dependent. The deepest minimum is obtained during the afternoon, when ultraviolet radiation near 2000 Å has photodissociated mesospheric nitric oxide. As solar zenith angle increases, the rate of NO photolysis decreases and the dip is progressively filled in by nitric oxide diffusing downward from the E-region.

In order to use a realistic NO variation between sunrise and sunset in the following simulations, an analytic formulation for the NO distribution between 100 and 150 km is adopted,

$$[\mathrm{NO}] = [A-(3.96\times10^4)-(1.6\times10^5)(z-115)^2]\times\left[1+B\sin\left(\frac{\pi}{9}(t-10.5)\right)\right]$$

for $z \leqslant 115$ km,

$$[\mathrm{NO}] = \left[A\exp\left(\frac{115-z}{30}\right)-(3.96\times10^4)\right]\times\left[1+B\sin\left(\frac{\pi}{9}(t-10.5)\right)\right] \quad (5)$$

for $z > 115$ km,

which are functions of altitude z(km) and time t(h), peaking at 115 km.

They describe a diurnal variation of NO concentration with a minimum in the early morning and a maximum around 15.00 LT, in agreement with the model calculation described above and satellite NO γ-band observations (STEWART and CRAVENS, 1978). The amplitude in these expressions is altitude-inde-

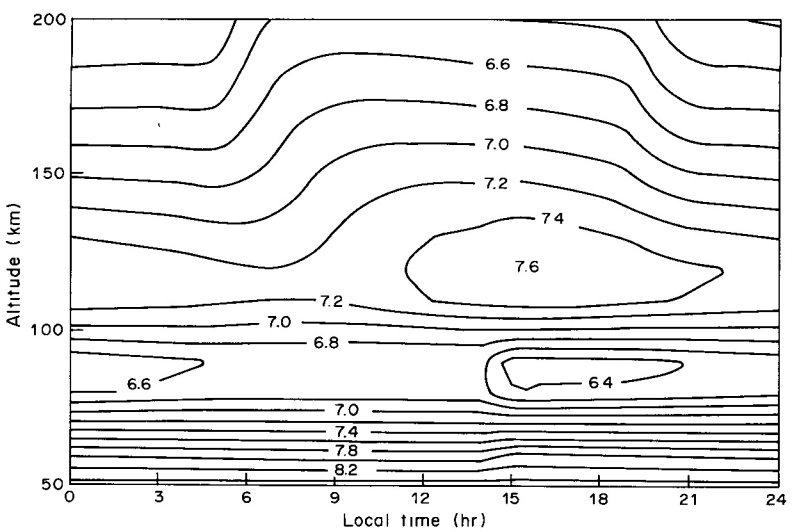

Fig. 5. Contour plot of the diurnal variation of $\log_{10}$ of the nitric oxide concentration calculated for the June 1978 observation period at Saint-Santin.

pendent, an approximation not valid below 100 km according to the NO model, which predicts no variation near 95 km and a reversed phase in the mesosphere. The amplitude of the diurnal variation and the NO concentration at 115 km may be modified. The NO model described above has been used to provide realistic values for parameters A and B controlling these quantities.

4. RESULTS OF THE IONOSPHERIC SIMULATIONS

Eight cases of the simulation for June 1978 are described in Table 4 which lists the values of several parameters of the calculations. The transport term of the continuity equation is neglected, except for case 8. The parameters which characterize the various cases are: the maximum NO concentration at 115 km, which corresponds to the altitude of the peak of the profile; the amplitude of the diurnal variation of NO characterized by the ratio of the [NO] maximum in the afternoon to the minimum in the morning; the MSIS temperature of the neutral constituents, which depends on local time ($T_n(t)$) or may be kept constant ($T_n = Ct$) at its initial value; the MSIS neutral concentrations, which vary with time ($[M(t)]$) or may be kept at a fixed value ($[M] = Ct$); the solar flux F_0, which is increased by 50% over the reference spectrum values for case 7.

The percentage morning–afternoon dissymmetry may be characterized by the quantity

$$\delta = 200\frac{N_e(\text{morning}) - N_e(\text{afternoon})}{N_e(\text{morning}) + N_e(\text{afternoon})}$$

for the particular value $\cos\chi = 0.78$. This value corresponds to 9.15 and 14.45 L.T. for 10 June at Saint-Santin.

Table 5 summarizes the results of the model simulations from 104.6 to 140.5 km for the 8 cases that differ according to the various values of the parameters of Table 4.

It has initially been checked that no asymmetry is obtained ($\delta = 0$) when [NO] is zero and T_n and the neutral concentrations are kept constant during the day. Secondly, diurnal variation of T_n and neutral concentrations is included as calculed by the MSIS model, whereas [NO] is set to zero. The results of case 1 show a rather complex behaviour. The dissymmetry is important at 104.6 km, but much less so at higher altitudes. It is even negative at two altitudes. This may be interpreted as due to the altitude dependence of the amplitude and phase of the diurnal variation of the neutral densities. For $\cos\chi = 0.78$, the concentrations of O, O_2 and N_2 are 26% higher in the afternoon than in the morning at 104.6 km; at 112.7 km the increase is 17.6% for O, 6.8% for O_2 and 3.6% for N_2. Since the reaction rates depend on both the neutral constituents and ion species, it is understandable that the behaviour is complex.

Cases (2) and (3) show the effect of nitric oxide only, since temperature and neutral composition are kept fixed in time. As expected, the diurnal variation of NO generates an N_e asymmetry for a few per cent, for the reasons described before. Increasing $[NO]_{max}$ from 4×10^7 to 5×10^8 cm^{-3} does not significantly modify the dissymmetry, except near 105 km, where it decreases from 4.7 to 2.1%.

Figure 6 corresponds to a more realistic situation (case 4) that includes simultaneously the NO time-dependence for a peak density of 4×10^7 cm^{-3} and an amplitude ratio of 2 and neutral atmosphere diurnal variation. This profile of nitric oxide is in close agreement with the results of the odd nitrogen calculations described above. The dissymmetry is more pronounced at 104.6 and 118.2 km than at intermediate altitudes. Above 118.3 km diurnal variation of the neutral concentrations tends to a few per cent, and even zero for N_2. In this region the role played by NO is dominant.

Figure 7 shows curves similar to Fig. 6 obtained for case 5, where [NO] is five times higher than case 4. The dissymmetry is somewhat more important at all

Table 4. Parameters used in the numerical simulations

	Case no.							
Parameter	1	2	3	4	5	6	7	8*
$[NO]_{max}$ (cm^{-3})	0	4×10^7	2×10^8	4×10^7	2×10^8	4×10^7	4×10^7	4×10^7
$[NO]_{max}/[NO]_{min}$		2	2	2	2	10	2	2
T_n	$T_n(t)$	$T_n = Ct$	$T_n = Ct$	$T_n(t)$	$T_n(t)$	$T_n(t)$	$T_n(t)$	$T_n(t)$
$[M]$	$[M](t)$	$[M] = Ct$	$[M] = Ct$	$[M](t)$	$[M](t)$	$[M](t)$	$[M](t)$	$[M](t)$
Solar flux	F_0	F_0	F_0	F_0	F_0	F_0	1.5 F_0	F_0

* Transport included in the electron continuity equation.

Table 5. Percentage variation δ of the electron density dissymmetry in the numerical simulations

	Case no.							
Altitude (km)	1	2	3	4	5	6	7	8
104.6	13.6	4.7	2.1	18.6	19.3	23.7	17.5	18.6
108.1	−1.6	4.4	5.6	1.8	4.1	7.5	1.3	1.7
112.7	−2.0	4.5	4.4	1.8	2.9	8.0	1.8	1.7
118.3	3.5	4.0	3.9	7.1	7.1	12.5	6.6	7.3
124.7	4.3	4.1	3.6	8.5	7.0	13.0	7.7	8.5
132.2	3.0	3.0	3.0	4.2	3.4	7.9	4.3	4.2
140.5	0	2.4	2.6	4.0	1.4	7.9	2.4	2.1

altitudes, but the electron density, regardless of solar zenith angle, is some 15% lower. This confirms that the amount of nitric oxide exerts an important control on the electron density.

Then, the value of [NO] is again set to $4 \times 10^7\,\mathrm{cm}^{-3}$ and relation (5) is modified to obtain a diurnal amplitude of 10 (case 6). The results are illustrated in Fig. 8. The electron density is not significantly altered compared to Fig. A1 but the dissymmetry is enhanced at all altitudes. Case 7, characterized by a solar flux 50% stronger than case 4, shows that the dissymmetry is slightly decreased at all altitudes except one. It indicates that the influence of the production rate of electrons on the magnitude of the asymmetry is marginal.

Finally, as expected, the inclusion of the transport term in the continuity equation has no noticeable effect on the dissymmetry (case 8).

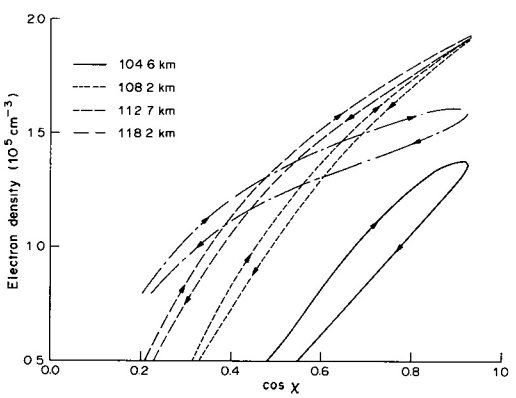

Fig. 6. Plot of electron density versus cos χ calculated for June 1978 at four different altitudes. The ascending arrows are for morning values, descending ones for the afternoon. The NO distribution adopted for the calculations peaks at $4 \times 10^7\,\mathrm{cm}^{-3}$, with a diurnal variation amplitude of 2.

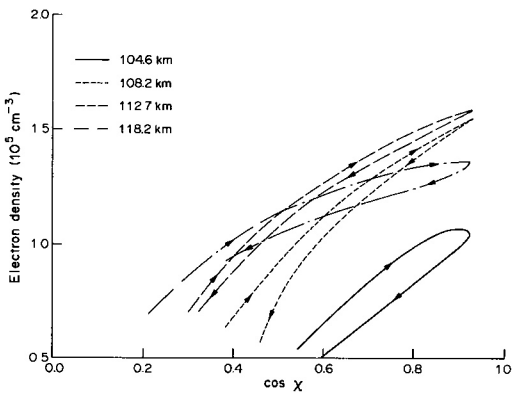

Fig. 7. As Fig. 6 with a peak NO concentration of $2 \times 10^8\,\mathrm{cm}^{-3}$.

5. DISCUSSION AND CONCLUSIONS

Dissymmetries about noon of *E*-region electron density have been observed in the past with ionosondes. However, this technique determines the *E*-

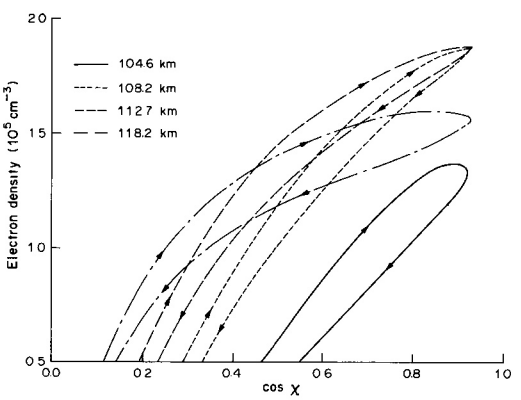

Fig. 8. As Fig. 6 with a peak NO concentration of $4 \times 10^7\,\mathrm{cm}^{-3}$ and a diurnal variation amplitude of 10.

region critical frequency, but cannot accurately provide the altitude of the measured N_e. Thus, small differences between morning and afternoon values could not be obtained reliably and led to erroneous interpretation. It is only with the use of incoherent scatter radars that this problem could be handled satisfactorily. So far, only Saint-Santin data have been used for this purpose.

In this study, based on observations made during 34 days at three different seasons, the existence of a diurnal dissymmetry in summer and winter has been clearly demonstrated. For most days, the morning values exceed the afternoon ones by 5–20%. In spring 1979 no significant asymmetry is observed. Numerical simulations using an ionospheric model taking into account the expected NO diurnal variation confirm the role of nitric oxide as suggested by Senior *et al.* (1981). The presence of NO converts part of the O_2^+ into NO^+, which recombines faster than O_2^+. Since NO is more abundant in the afternoon, the electron density is reduced compared to the morning values, in agreement with the observations. The calculated amplitude of the dissymmetry depends both on the NO average concentration and the amplitude of its diurnal variation. Dissymmetries of the order of 5% are predicted for the expected summer diurnal variation over Saint-Santin. The effect of changes of the neutral concentrations and composition, as given by the MSIS-1983 model, has been investigated in the simulations. This effect appears complex and altitude-dependent. For example, above 115 km morning N_e values exceed the afternoon ones by 3–4%, but a reversed trend is predicted at lower altitude. This complex behaviour results from the combination of diurnal changes in local concentration and variations in solar radiation absorption by the overlying atmosphere. These two factors act in opposite directions and partly compensate each other. The magnitude of this compensation depends on the optical depth, and thus on altitude.

When both effects are considered the resulting amplitude of the dissymmetry is not the addition of the two separate contributions, as shown by the numerical model. The total amplitude is between 3 and 20% and does not vary uniformly with altitude. This is in general qualitative and quantitative agreement with most of the observations.

The numerical simulation is based on neutral and NO models describing average values of the concentrations, which do not correspond to instantaneous local conditions. Consequently, the model cannot reproduce in detail the actual measurements. The measurements around 7 June 1978 are a remarkable illustration of a behaviour which is noticeably different from the average. The amplitude of the dissymmetry reaching nearly 50% and the presence of a noon minimum are unusual features. However, the data for 28 April 1970, discussed by Monro *et al.* (1976), also exhibit a very large dissymmetry, reaching about a factor of 2.

The absolute upper limit (36%) of the dissymmetry due to nitric oxide is given by

$$\sqrt{\frac{\alpha_4}{\alpha_2}} = 1.36,$$

corresponding to an ionosphere composed exclusively of NO^+ or O_2^+. Consequently, NO is not the only factor contributing to this exceptionally large effect. It is possible that the *E*-region neutral composition may be seriously perturbed, possibly as a consequence of the major magnetic storm which developed a few days earlier.

So far, the emphasis has been put on the June 1978 data, the longest of the three periods of observations. Table 2 exhibits seasonal differences in the value of $\bar{R}$ and its standard deviation.

The larger variability of the winter asymmetry ratio at 100 km compared to 120 km and to other seasons at 105 km is an interesting feature of Table 2. A reasonable quantitative explanation lies in the greater variability of NO in winter than in other seasons. Indeed, satellite measurements made during solar cycle minimum (Cravens and Stewart, 1978) showed a larger variability of NO peak concentration at the latitude of Saint-Santin in winter than in summer. This is probably caused by equatorward propagation of large NO enhancements generated by particle ionization in the auroral zone. The existence of the *D*-region winter anomalous absorption is further indirect evidence for winter NO variability. The winter anomaly is usually separated into two components: the 'regular' and the 'irregular' components. The latter is characterized by periods of a few days with large absorption. It is more transient in nature than the regular component and probably results from the addition of several effects, as demonstrated during the *D*-region winter anomaly campaign 1975–1976. Analysis of time and spatial scales involved in this phenomenon led Offermann *et al.* (1982) to conclude that the existence of regions with stronger vertical turbulent transport is the best candidate to explain the spikes in absorption. In this picture, thermospheric NO molecules would be rapidly carried downward into the *D*-region over time scales of the order of a fraction of a day and may possibly affect the *E*-region concentration, especially below the NO peak. Thus, although a day-to-day correlation with winter

anomaly events is outside the scope of this study, the existence of the anomaly in itself is consistent with a larger variability of nitric oxide at mid-latitudes during winter months than other periods. The fact that the asymmetry ratio $\bar{R}$ is over 3 times larger at 100 than at 120 km is also consistent with this picture.

The lack of statistical asymmetry in the March 1979 observations is more puzzling. The NO time-dependent model predicts a behaviour similar to the June period, with a slightly reduced amplitude of the peak and a somewhat different phase. The ionospheric model also gives *E*-region asymmetries similar to those listed in Table 5. The absence of asymmetry is possibly non-typical of other equinoctial periods. Indeed, as mentioned in Section 2, the period was characterized by the onset of a geomagnetic storm on 22 March at 8.30 UT. A description of other Saint-Santin measurements made during this storm has been given by TAIEB and POINSARD (1984b), who found that the *F*-region electron density collapsed during the night of 22–23 March. The following days were characterized by the presence of strong winds blowing southward in the *F*-region and northward in the *E*-region. It is possible that these disturbed conditions perturbed the normal diurnal variation of both the major constituents and nitric oxide and counteracted the normal *E*-region dissymmetry. Unfortunately, no other similar period of consecutive equinoctial measurements exists in the Saint-Santin data base to determine whether the March behaviour may be considered as typical. Future observations with incoherent scatter facilities of the *E*-region equinoctial electron density would be needed to solve this question.

Acknowledgements—We are grateful to M. LAFEUILLE (CNET-CNRS/CRPE) for her contribution to the data analysis. The ionospheric simulation was performed on a CRAY-1 computer thanks to funds provided by the Scientific Council of CCVR. J. C. GÉRARD is supported by the Belgian National Foundation for Scientific Research (FNRS). Financial support by FRFC grant No. 2.4507.82 is also acknowledged.

REFERENCES

APPLETON E.V.	1953	*J. atmos. terr. Phys.* **3,** 282.
APPLETON E. V. and LYON A. J.	1961	*J. atmos. terr. Phys.* **21,** 73.
CRAVENS T. E., GÉRARD J. C., STEWART A. I. and RUSCH, D. W.	1979	*J. geophys. Res.* **84,** 2675.
EBEL A.	1980	*J. atmos. terr. phys.* **42,** 617.
FORBES J. M.	1981	*J. geophys. Res.* **86,** 1551.
FREDERICK J. E. and HUDSON R. D.	1979	*J. atmos. Sci.* **36,** 737.
HEDIN A. E.	1983	*J. geophys. Res.* **88,** 10170.
LEAN J. L., WHITE O. R., LIVINGSTON W. C., HEATH D. F., DONNELLY R. F. and SKUMANICH A.	1982	*J. geophys. Res.* **87,** 10307.
MAZAUDIER C. and BERNARD R.	1985	*J. geophys. Res.* **90,** 2885.
MONRO P. E., NISBET J. S. and STICK T. L.	1976	*J. atmos. terr. Phys.* **38,** 523.
OFFERMANN D., BRÜCKELMANN H. G. K., BARNETT J. J., LABITZKE K., TORKAR K. M. and WIDDEL H. U.	1982	*J. geophys. Res.* **87,** 8286.
ORAN E. S., JULIENNE P. S. and STROBEL D. F.	1975	*J. geophys. Res.* **80,** 3068.
PANDEY V. K. and MAHAJAN K. K.	1981	*Indian J. Radio Space Phys.* **10,** 85.
RUSCH D. W., STEWART A. I., HAYS P. B. and HOFFMAN J. H.	1975	*J. geophys. Res.* **80,** 2300.
SAMAIN D. and SIMON P. C.	1976	*Solar Phys.* **49,** 33.
SENIOR C., BAUER P., TAIEB C. and PETIT M.	1981	*C.r. hebd. Séanc. Acad. Sci., Paris* **292,** 1195.
STEWART A. I.	1970	*J. geophys. Res.* **75,** 6333.
STEWART A. I. and CRAVENS T. E.	1978	*J. geophys. Res.* **83,** 2453.
TAIEB C. and POINSARD P.	1984a	*Annls Géophys.* **2,** 197.
TAIEB C. and POINSARD P.	1984b	*Annls Géophys.* **2,** 359.
TORR M. R. and TORR D. G.	1982	*Rev. Geophys. Space Phys.* **20,** 91.
TORR M. R., TORR D. G., ONG R. A. and HINTEREGGER H. E.	1979a	*Geophys. Res. Lett.* **6,** 771.
TORR D. G., TORR M. R., BRINTON H. C., BRACE L. H., SPENCER N. W., HEDIN A. E., HANSON W. B., HOFFMAN J. H., NIER A. O., WALKER J. C. G. and RUSCH D. W.	1979b	*J. geophys. Res.* **84,** 3360.

APPENDIX. THE NO TIME-DEPENDENT MODEL

The model solves the coupled time-dependent continuity equations

$$\frac{\partial n_i}{\partial t} = P_i - v_i n_i - \frac{\partial \phi_i}{\partial z} \tag{1}$$

and the flux equations

$$\phi_i = -D_i\left(\frac{n_i}{H_i} + \frac{\partial n_i}{\partial z} + n_i\frac{\partial \ln T}{\partial z}\right) - K\left(\frac{n_i}{\bar{H}} + \frac{\partial n_i}{\partial z} + n_i\frac{\partial \ln T}{\partial z}\right), \tag{2}$$

for NO and N(^4S) between 50 and 250 km. In these equations, n_i is the NO or N(^4S) concentration, D_i the molecular diffusion coefficient, H_i the diffusive equilibrium scale height and $\bar{H}$ the background atmospheric scale height.

Photochemical equilibrium is assumed for N(^2D), N_2^+, O_2^+, $O^+(^4S)$, $O^+(^2D)$, $O^+(^2P)$, NO^+, N^+ and electrons. The temperature and the major constituent vertical distribution above 85 km are given by the MSIS 1983 model (HEDIN, 1983). Below this altitude the U.S. Standard Atmosphere (1976) temperature profile is smoothly connected to the MSIS value at 85 km and the concentrations of N_2 and O_2 are calculated by integrating downward the hydrostatic equilibrium equations. The atomic oxygen distribution is obtained by merging the initial profile with the value given by MSIS at 85 km. A system of two parabolic partial differential equations is obtained by combining (1) and (2),

$$\frac{\partial n_i}{\partial t} = A_i\frac{\partial^2 n_i}{\partial z^2} + B_i\frac{\partial n_i}{\partial z} + C_i n_i + E_i, \tag{3}$$

where

$$A_i = D_i + K,$$

$$B_i = \frac{\partial}{\partial z}(D_i + K) + (D_i + K)\frac{\partial \ln T}{\partial z} + \frac{D_i}{H_i} + \frac{K}{\bar{H}},$$

$$C_i = (D_i + K)\frac{\partial^2 \ln T}{\partial z^2} + \frac{\partial \ln T}{\partial z}\frac{\partial}{\partial z}(D_i + K) + \frac{1}{H_i}\frac{\partial D_i}{\partial z} + \frac{1}{\bar{H}}\frac{\partial K}{\partial z} - \frac{D_i}{H_i^2}\frac{\partial H_i}{\partial z} - \frac{K}{\bar{H}^2}\frac{\partial \bar{H}}{\partial z} - v_i,$$

$$E_i = P_i.$$

The system of partial differential equations (3) with appropriate boundary conditions is solved by the finite element method. The spatial mesh size varies with the altitude: 2.5 km between 50 and 125 km, 5 km between 125 and 180 km and 10 km above 180 km. The time step size is adjusted automatically by the integrator to ensure adequate convergence and accuracy. Periodically the local time is incremented, the production and loss terms P_i and v_i and the photochemical densities are updated and the solver computes new values for n_i. These solutions are, in turn, used as new initial conditions and iterations over local time intervals are carried out until the desired final time is reached. The local time intervals of the iterations are progressively increased up to a specified maximum value. This value is decreased to a few minutes at periods of sunrise and sunset when the chemical production and loss terms change fairly rapidly. Dirichlet conditions are used for both species at the lower boundary. A value of 3×10^8 cm^{-3} is assumed for NO, in agreement with observations of NO near the stratopause. Due to the short photochemical lifetime of N(^4S) at the lower boundary, the N(^4S) concentration is set equal to its photochemical value. At the upper boundary N and NO are nearly in diffusive equilibrium and a zero flux condition is used for both constituents.

The reactions affecting odd nitrogen and their rate coefficients are listed in Table 3 and the reaction scheme controlling thermospheric odd nitrogen is plotted in Fig. A1. Most of the rate coefficients used in this model are from TORR *et al.* (1979a) and TORR and TORR (1982). The altitude dependence of the ionization coefficients is parameterized following the expressions given by STEWART (1970). The unattenuated ionization frequencies are derived from the detailed calculations by TORR *et al.* (1979a) based on EUV solar fluxes measured by the AE satellites at various phases of the solar cycle. A linear fit to the calculated values is used to parameterize the dependence on solar activity level represented by the $F_{10.7}$ flux index. The fraction f of N(^2D) atoms produced by electron impact and photodissociation of N_2 is taken as 0.7 in this study.

The partition of O^+ ions between the ^4S, ^2D and ^2P terms is also made according to calculations by TORR *et al.* (1979b). The ionization rates of N_2, O_2 and O by photoelectrons are assumed to be fractions of the ionization by EUV photons. The values of these fractions have been summarized by TORR and TORR (1979b).

The dissociation rates of NO by predissociation in the (1, 0) and (0, 0) δ-bands at 1827 and 1920 Å, respectively, have been calculated in detail by FREDERICK and HUDSON (1979). A weak dependence of J_{NO} on solar activity is introduced by the variability of the solar irradiance near 2000 Å over a solar cycle. Since no reliable observations at these wavelengths exist over a sufficient time period, we use the results

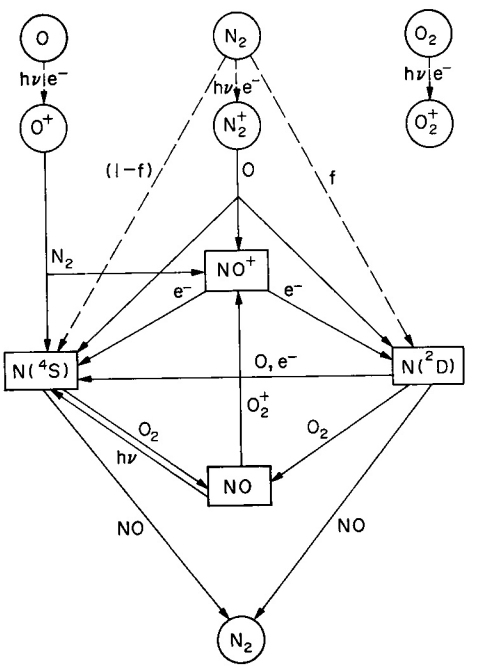

Fig. A1. Block diagram of processes controlling thermospheric odd nitrogen. Dotted lines indicate processes involving nonthermal particles (electrons or photons).

anomaly events is outside the scope of this study, the existence of the anomaly in itself is consistent with a larger variability of nitric oxide at mid-latitudes during winter months than other periods. The fact that the asymmetry ratio $\bar{R}$ is over 3 times larger at 100 than at 120 km is also consistent with this picture.

The lack of statistical asymmetry in the March 1979 observations is more puzzling. The NO time-dependent model predicts a behaviour similar to the June period, with a slightly reduced amplitude of the peak and a somewhat different phase. The ionospheric model also gives *E*-region asymmetries similar to those listed in Table 5. The absence of asymmetry is possibly non-typical of other equinoctial periods. Indeed, as mentioned in Section 2, the period was characterized by the onset of a geomagnetic storm on 22 March at 8.30 UT. A description of other Saint-Santin measurements made during this storm has been given by TAIEB and POINSARD (1984b), who found that the *F*-region electron density collapsed during the night of 22–23 March. The following days were characterized by the presence of strong winds blowing southward in the *F*-region and northward in the *E*-region. It is possible that these disturbed conditions perturbed the normal diurnal variation of both the major constituents and nitric oxide and counteracted the normal *E*-region dissymmetry. Unfortunately, no other similar period of consecutive equinoctial measurements exists in the Saint-Santin data base to determine whether the March behaviour may be considered as typical. Future observations with incoherent scatter facilities of the *E*-region equinoctial electron density would be needed to solve this question.

Acknowledgements—We are grateful to M. LAFEUILLE (CNET-CNRS/CRPE) for her contribution to the data analysis. The ionospheric simulation was performed on a CRAY-1 computer thanks to funds provided by the Scientific Council of CCVR. J. C. GÉRARD is supported by the Belgian National Foundation for Scientific Research (FNRS). Financial support by FRFC grant No. 2.4507.82 is also acknowledged.

REFERENCES

APPLETON E.V.	1953	*J. atmos. terr. Phys.* **3,** 282.
APPLETON E. V. and LYON A. J.	1961	*J. atmos. terr. Phys.* **21,** 73.
CRAVENS T. E., GÉRARD J. C., STEWART A. I. and RUSCH, D. W.	1979	*J. geophys. Res.* **84,** 2675.
EBEL A.	1980	*J. atmos. terr. phys.* **42,** 617.
FORBES J. M.	1981	*J. geophys. Res.* **86,** 1551.
FREDERICK J. E. and HUDSON R. D.	1979	*J. atmos. Sci.* **36,** 737.
HEDIN A. E.	1983	*J. geophys. Res.* **88,** 10170.
LEAN J. L., WHITE O. R., LIVINGSTON W. C., HEATH D. F., DONNELLY R. F. and SKUMANICH A.	1982	*J. geophys. Res.* **87,** 10307.
MAZAUDIER C. and BERNARD R.	1985	*J. geophys. Res.* **90,** 2885.
MONRO P. E., NISBET J. S. and STICK T. L.	1976	*J. atmos. terr. Phys.* **38,** 523.
OFFERMANN D., BRÜCKELMANN H. G. K., BARNETT J. J., LABITZKE K., TORKAR K. M. and WIDDEL H. U.	1982	*J. geophys. Res.* **87,** 8286.
ORAN E. S., JULIENNE P. S. and STROBEL D. F.	1975	*J. geophys. Res.* **80,** 3068.
PANDEY V. K. and MAHAJAN K. K.	1981	*Indian J. Radio Space Phys.* **10,** 85.
RUSCH D. W., STEWART A. I., HAYS P. B. and HOFFMAN J. H.	1975	*J. geophys. Res.* **80,** 2300.
SAMAIN D. and SIMON P. C.	1976	*Solar Phys.* **49,** 33.
SENIOR C., BAUER P., TAIEB C. and PETIT M.	1981	*C.r. hebd. Séanc. Acad. Sci., Paris* **292,** 1195.
STEWART A. I.	1970	*J. geophys. Res.* **75,** 6333.
STEWART A. I. and CRAVENS T. E.	1978	*J. geophys. Res.* **83,** 2453.
TAIEB C. and POINSARD P.	1984a	*Annls Géophys.* **2,** 197.
TAIEB C. and POINSARD P.	1984b	*Annls Géophys.* **2,** 359.
TORR M. R. and TORR D. G.	1982	*Rev. Geophys. Space Phys.* **20,** 91.
TORR M. R., TORR D. G., ONG R. A. and HINTEREGGER H. E.	1979a	*Geophys. Res. Lett.* **6,** 771.
TORR D. G., TORR M. R., BRINTON H. C., BRACE L. H., SPENCER N. W., HEDIN A. E., HANSON W. B., HOFFMAN J. H., NIER A. O., WALKER J. C. G. and RUSCH D. W.	1979b	*J. geophys. Res.* **84,** 3360.

APPENDIX. THE NO TIME-DEPENDENT MODEL

The model solves the coupled time-dependent continuity equations

$$\frac{\partial n_i}{\partial t} = P_i - v_i n_i - \frac{\partial \phi_i}{\partial z} \tag{1}$$

and the flux equations

$$\phi_i = -D_i\left(\frac{n_i}{H_i} + \frac{\partial n_i}{\partial z} + n_i\frac{\partial \ln T}{\partial z}\right) - K\left(\frac{n_i}{\bar{H}} + \frac{\partial n_i}{\partial z} + n_i\frac{\partial \ln T}{\partial z}\right), \tag{2}$$

for NO and N(^4S) between 50 and 250 km. In these equations, n_i is the NO or N(^4S) concentration, D_i the molecular diffusion coefficient, H_i the diffusive equilibrium scale height and $\bar{H}$ the background atmospheric scale height.

Photochemical equilibrium is assumed for N(^2D), N_2^+, O_2^+, $O^+(^4S)$, $O^+(^2D)$, $O^+(^2P)$, NO^+, N^+ and electrons. The temperature and the major constituent vertical distribution above 85 km are given by the MSIS 1983 model (HEDIN, 1983). Below this altitude the U.S. Standard Atmosphere (1976) temperature profile is smoothly connected to the MSIS value at 85 km and the concentrations of N_2 and O_2 are calculated by integrating downward the hydrostatic equilibrium equations. The atomic oxygen distribution is obtained by merging the initial profile with the value given by MSIS at 85 km. A system of two parabolic partial differential equations is obtained by combining (1) and (2),

$$\frac{\partial n_i}{\partial t} = A_i\frac{\partial^2 n_i}{\partial z^2} + B_i\frac{\partial n_i}{\partial z} + C_i n_i + E_i, \tag{3}$$

where

$$A_i = D_i + K,$$

$$B_i = \frac{\partial}{\partial z}(D_i+K) + (D_i+K)\frac{\partial \ln T}{\partial z} + \frac{D_i}{H_i} + \frac{K}{\bar{H}},$$

$$C_i = (D_i+K)\frac{\partial^2 \ln T}{\partial z^2} + \frac{\partial \ln T}{\partial z}\frac{\partial}{\partial z}(D_i+K) + \frac{1}{H_i}\frac{\partial D_i}{\partial z} + \frac{1}{\bar{H}}\frac{\partial K}{\partial z} - \frac{D_i}{H_i^2}\frac{\partial H_i}{\partial z} - \frac{K}{\bar{H}^2}\frac{\partial \bar{H}}{\partial z} - v_i,$$

$$E_i = P_i.$$

The system of partial differential equations (3) with appropriate boundary conditions is solved by the finite element method. The spatial mesh size varies with the altitude: 2.5 km between 50 and 125 km, 5 km between 125 and 180 km and 10 km above 180 km. The time step size is adjusted automatically by the integrator to ensure adequate convergence and accuracy. Periodically the local time is incremented, the production and loss terms P_i and v_i and the photochemical densities are updated and the solver computes new values for n_i. These solutions are, in turn, used as new initial conditions and iterations over local time intervals are carried out until the desired final time is reached. The local time intervals of the iterations are progressively increased up to a specified maximum value. This value is decreased to a few minutes at periods of sunrise and sunset when the chemical production and loss terms change fairly rapidly. Dirichlet conditions are used for both species at the lower boundary. A value of 3×10^8 cm^{-3} is assumed for NO, in agreement with observations of NO near the stratopause. Due to the short photochemical lifetime of N(^4S) at the lower boundary, the N(^4S) concentration is set equal to its photochemical value. At the upper boundary N and NO are nearly in diffusive equilibrium and a zero flux condition is used for both constituents.

The reactions affecting odd nitrogen and their rate coefficients are listed in Table 3 and the reaction scheme controlling thermospheric odd nitrogen is plotted in Fig. A1. Most of the rate coefficients used in this model are from TORR *et al.* (1979a) and TORR and TORR (1982). The altitude dependence of the ionization coefficients is parameterized following the expressions given by STEWART (1970). The unattenuated ionization frequencies are derived from the detailed calculations by TORR *et al.* (1979a) based on EUV solar fluxes measured by the AE satellites at various phases of the solar cycle. A linear fit to the calculated values is used to parameterize the dependence on solar activity level represented by the $F_{10.7}$ flux index. The fraction f of N(^2D) atoms produced by electron impact and photodissociation of N_2 is taken as 0.7 in this study.

The partition of O^+ ions between the ^4S, ^2D and ^2P terms is also made according to calculations by TORR *et al.* (1979b). The ionization rates of N_2, O_2 and O by photoelectrons are assumed to be fractions of the ionization by EUV photons. The values of these fractions have been summarized by TORR and TORR (1979b).

The dissociation rates of NO by predissociation in the (1, 0) and (0, 0) δ-bands at 1827 and 1920 Å, respectively, have been calculated in detail by FREDERICK and HUDSON (1979). A weak dependence of J_{NO} on solar activity is introduced by the variability of the solar irradiance near 2000 Å over a solar cycle. Since no reliable observations at these wavelengths exist over a sufficient time period, we use the results

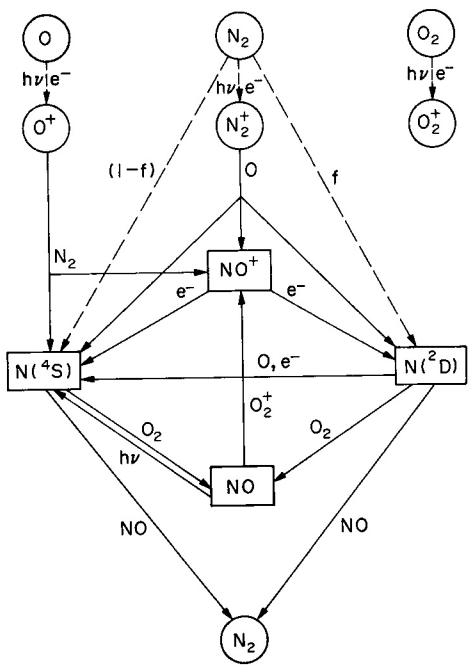

Fig. A1. Block diagram of processes controlling thermospheric odd nitrogen. Dotted lines indicate processes involving non-thermal particles (electrons or photons).

of the three component model of LEAN *et al.* (1982), which predicts a ratio between solar maximum and minimum of the order of 20%. Besides, the unattenuated dissociation frequency calculated by Frederick and Hudson needs to be first normalized to the solar irradiance reported by SAMAIN and SIMON (1976), considered as representative of solar minimum conditions. The expression adopted for the dissociation frequency of nitric oxide outside the atmosphere is

$$J_{NO}^{\infty} = 4.6 \times 10^{-6}[1+(F_{10.7}-75)/263]\,s^{-1}, \quad (4)$$

where $F_{10.7}$ is the solar flux at 10.7 cm in $10^{-22}\,W\,m^{-2}\,Hz^{-1}$. Besides EBEL's (1980) latitude-dependent eddy diffusion coefficients, the low K coefficient given by ORAN *et al.* (1975),

$$K = \begin{cases} 1\times10^{6}\ cm^{2}\,s^{-1} & z \geqslant 100\ km, \\ 1\times10^{6}\exp\left(-\dfrac{Z-100}{2\bar{H}}\right) cm^{2}\,s^{-1} & z < 100\ km, \end{cases}$$

has also been used for comparison (Fig. 4).